Journal of Applied Electrochemistry (2025) 55:3235–3246
https://doi.org/10.1007/s10800-025-02378-y

RESEARCH ARTICLE

# On the role of cysteamine modification of gold electrodes in redox reactions with dopamine

**H. Caparrotti**[1] · **Y. E. Silina**[1]

Received: 9 July 2025 / Accepted: 27 September 2025 / Published online: 16 October 2025


**Abstract** While cysteamine (CystAm) is widely used for forming thiol-based self-assembled monolayers on gold electrodes in biosensor applications, its broader influence on dopamine (DA) sensing mechanisms remains underexplored. This study re-evaluates the impact of CystAm on both electrochemical and biochemical reactions involving DA. Using model electrochemical experiments supported by X-ray photoelectron spectroscopy, oxygen mini-sensor, and quartz crystal microbalance studies, it was shown that CystAm primarily suppresses the gold electrode's oxygen reduction reaction, thereby altering non-enzymatic DA redox behavior. In contrast, it does not significantly affect enzyme immobilization, retained mass, elution rates, or enzymatic activity on the electrode surface. Based on this knowledge, a CystAm-modified gold electrode functionalized with a tyrosinase–chitosan biosensing layer was produced. The resulting electrode was evaluated in artificial saliva spiked with low concentrations of DA. It exhibited high reliability, achieving average DA recovery rates of 99–100% with precision values < 10%, demonstrating its potential for accurate analysis in biological samples.

**Graphical abstract**

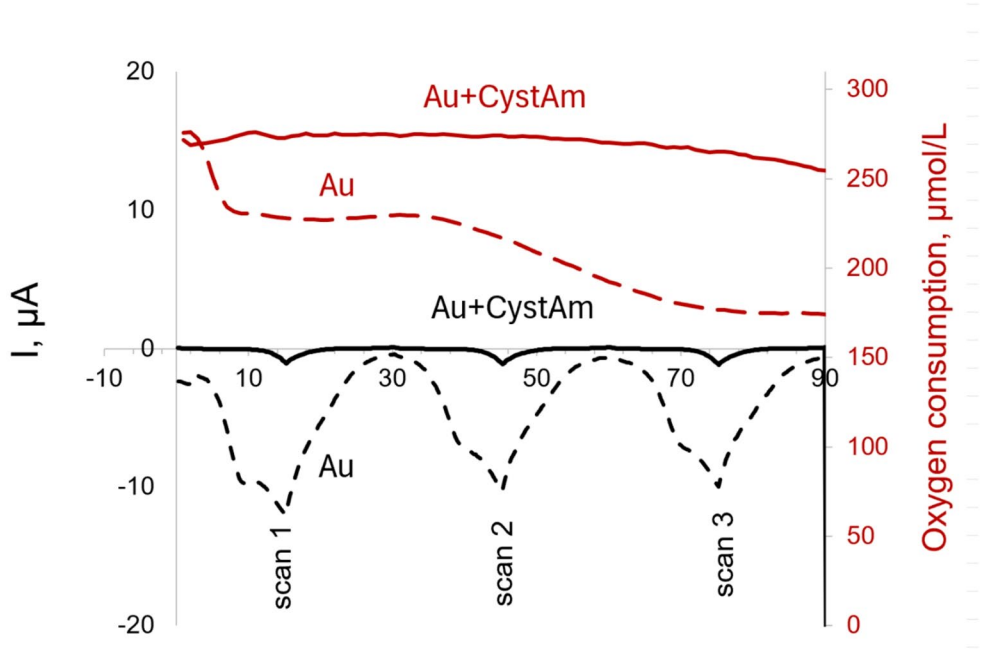


**Keywords** Gold · Cysteamine · Oxygen reduction reaction · Dopamine · Tyrosinase

✉ Y. E. Silina
yuliya.silina@gmx.de; yuliya.silina@uni-saarland.de

[1] Institute of Biochemistry, Saarland University, Campus B 2.2, Saarbrücken, Germany

**Abbreviations**

| | |
|---|---|
| SPE | Screen printed electrodes |
| Au-AT (Au) | Gold electrodes |
| CystAm | Cysteamine |
| Tyr | Tyrosinase |
| CS | Chitosan |
| DA | Dopamine |
| DQ | Dopamine-quinone |
| LbL | Layer by layer |
| SAM | Self-assembled monolayer |
| QCM | Quartz microbalance |
| CV | Cyclic voltammetry |
| AM | Amperometry |
| SEM | Scanning Electron Microscopy |
| XPS | X-ray photoelectron spectroscopy |
| ESI-MS | Electrospray ionization mass spectrometry |
| LDR | Linear dynamic range |
| LOQ | Limit of quantification |
| ORR | Oxygen reduction reaction |

## 1 Introduction

Dopamine (DA) is a low molecular weight compound that belongs to the class of neurotransmitters and plays a vital role in various physiological processes. A deficiency in DA has been associated to several medical conditions, including depression, Parkinson's, Alzheimer´s diseases, and attention deficit hyperactivity disorder [1]. The primary cause of Parkinson's disease is the degeneration of DA-producing neurons in the brain. As DA levels decrease, the brain's ability to regulate movement deteriorates. To mitigate these symptoms, L-DOPA, a DA precursor, is administered to help restore DA levels [2]. However, optimizing L-DOPA dosage, balancing therapeutic effects, and monitoring treatment efficacy require reliable analytical methods capable of accurately and rapidly quantifying DA levels in real biological matrices (e.g., saliva, serum, or urine) at micromolar (μM) concentrations.

Currently, the analysis of DA-related compounds relies primarily on ultra-performance liquid chromatography coupled with tandem mass spectrometry (UPLC-MS/MS), a technique that is complex, time consuming, and requires extensive sample preparation and compound separation [3, 4]. To overcome these limitations, fluorescent, enzymatic and non-enzymatic electrochemical biosensors have been developed for determination of DA in model and real biological matrices [5–7].

In most cases, non-enzymatic electrochemical sensing of DA lacks specificity in complex media containing other electroactive compounds [6, 7]. Enzymatic-based electrochemical DA biosensors are primarily based on enzymes containing copper cofactors such as tyrosinase or laccase, which are immobilized on a transducer surface [8, 9]. When DA comes into contact with the enzyme, it undergoes oxidation, and this reaction is coupled to a measurable electrical signal. The generated dopamine-o-quinone (as a product of enzymatic reaction) can then be electrochemically detected at a lower potential, minimizing interference from other electroactive compounds. The main limitation of enzymatic DA biosensors lies in the rapid leaching of the water-soluble biosensing recognition element (the enzyme) from the electrode surface, finally leading to a loss of biosensor/electrode activity.

To address this issue, cysteamine (CystAm) treatment was proposed prior to enzyme immobilization on the electrode surface. The attachment of CystAm molecules to the surface enables the subsequent functionalization and manipulation of the modified surface for various applications. CystAm modification is commonly used in biosensor applications for electrode surface functionalization, enabling the formation of self-assembled monolayers (SAMs) or layer-by-layer (LbL) assemblies [10–12].

Regardless of the electrode type (copper, silver, gold, etc.), CystAm treatment is considered beneficial for attaching biomolecules in the correct/preferred orientation and binding them more closely and reliably to the electrode surface [13–15]. CystAm-coated noble or transition metal electrodes are positively charged as synthesized and can therefore interact with negatively charged enzymes, for example, tyrosinase (Tyr) from mushrooms, which has an isoelectric point of approximately 4.4–4.9 [16]. To sum it up, CystAm is considered to function as a molecular linker that facilitates enzyme immobilization and retention on electrode surfaces.

At the same time, its role in modifying the electrocatalytic properties of electrodes in redox reactions involving electroactive neurotransmitters, such as DA, cannot be excluded. In this case the tailoring of electroanalytical responses of biosensors can simply be achieved by altering the properties of the inorganic component/electrocatalyst while maintaining a constant amount of the biosensing layer (enzyme).

The goal of this study was to re-investigate the role of CystAm modification of gold electrodes (electrocatalysts) in redox reactions involving low concentrations of DA, using model electrochemical experiments and a combination of advanced analytical methods. The obtained results clearly indicate that CystAm is more likely to influence the electroanalytical performance of the gold electrocatalyst toward DA, rather than affect the architecture or properties of the enzymatic biosensing layer. More specifically, modification of the gold electrode with CystAm

suppresses its activity toward the oxygen reduction reaction (ORR), thereby improving the specificity of enzymatic DA detection.

## 2 Experimental part

### 2.1 Chemicals and materials

Screen-printed electrodes (SPEs) modified with a gold layer (Au-AT, a sputtered gold thin film on the working electrode; counter electrode –Au; reference electrode –Ag/AgCl) were obtained from DropSens (Metrohm, Germany).

Cysteamine, catechol oxidase (tyrosinase, Tyr) from mushroom (lyophilized powder, 50000 units/mg), medium molecular weight chitosan (CS), acetic acid, 98% dopamine hydrochloride, 99% hydroquinone, ascorbic acid, glucose, L-lactate, EtOH, 35% hydrogen peroxide solution ($H_2O_2$), artificial saliva (Fusayama/Meyer artificial saliva) were received from Merck (Darmstadt, Germany).

### 2.2 Modification of gold electrodes with cysteamine (CystAm)

The Au-AT SPEs were used without any pre-cleaning steps in order to preserve their original surface chemistry and morphology. This was essential to ensure reproducible surface modification with CystAm, and reliable subsequent immobilization of the Tyr-based biosensing layer (see Sect. 2.3).

3 µL of 20 mM CystAm, prepared in a 3:1 *v/v* EtOH/$H_2O$ mixture was drop-coated onto the working gold electrode (Au-AT) and then stored for 12 h. After this period, the electrode was rinsed with DI water to remove any remaining unbound thioamine.

### 2.3 Formation of the sensing layer containing tyrosinase (Tyr) and chitosan (CS)

Cysteamine acts as a "cross-linker" between the gold electrode and the immobilized enzyme. On one side, it binds to the gold surface through the formation of a thiol–gold bond, anchoring it to the electrode. On the other side, the amino group in the CystAm structure facilitates enzyme attachment, leading to the formation of a self-assembled monolayer (SAM) [10, 15].

Next, for Tyr immobilization on the working gold electrode, a Tyr solution (11 mg/mL) was prepared in phosphate buffer (pH 5.4 ± 0.2), and 3 µL was dropped onto the CystAm-modified gold electrode, then allowed to dry at 4 °C for 40–50 min. The pH of test solutions was monitored by a Horiba LAQUAtwin pH meter pH-22 (Neomeris, France).

A 2% chitosan (CS) solution was prepared by dissolving 0.309 g of CS in 15 mL of a 1% (*v/v*) acetic acid solution, followed by stirring for 24 h. Subsequently, 3 µL of the freshly prepared chitosan solution was applied to the CystAm-modified gold electrode with immobilized Tyr and allowed to dry at 4 °C for 24 h. The architecture of the resulting LbL sensing film is summarized in ESI, Fig. S1. Following the drying step, the electrode was gently rinsed with deionized (DI) water to remove any unbound or unreacted compounds.

As a reference system, an unmodified gold electrode was prepared by sequentially drop-coating it with Tyr and CS, hereafter referred to as the "Tyr-CS biosensing layer", following the same procedure described above. All freshly prepared electrodes with biosensing layers were stored at 4 °C until use.

### 2.4 Quartz microbalance (QCM) studies

To clarify the impact of CystAm modification on the architecture of the biosensing layers, a QCM 200 system (SRS, Scientific Instruments GmbH, Gilching, Germany) was employed. This technique enables the detection of subtle changes in film architecture at the nanogram (ng) or microgram (µg) level. If CystAm modification significantly influences enzyme attachment to the gold surface by altering factors such as protein conformation, orientation, or packing density or affects the retention of the deposited Tyr-CS biosensing layer, corresponding shifts in resonance frequency would be expected.

For the experiments, the biosensing layer architectures formed on both unmodified and CystAm-modified gold electrodes (see Sect. 2.3) were reconstituted on the surface of gold-coated quartz piezoelectric crystals with a fundamental frequency of 5 MHz. The corresponding frequency shifts (in Hz) were then recorded to evaluate changes in mass deposition.

The Sauerbrey model [17] was used to calculate the total mass change:

$$\Delta m = -\frac{\Delta f}{\mathrm{C}} \cdot A, \tag{1}$$

where Δf is the defined frequency shift, Hz; C is the mass sensitivity constant (for 5 MHz AT-cut quartz, C ≈ 17.7 ng/Hz·cm$^2$; A is the electrode area (5.06 cm$^2$).

In a simplified form this formula can be summarised as follows:

$$m \approx -17.7 \cdot 5.06 \cdot \Delta f \tag{2}$$

Changes in mass (µg) of the QCM crystals were monitored following the preparation of the biosensing layers on both electrodes (see Sect. 2.3). The measured frequency shifts reflect the immobilized mass (µg) of the biosensing layers. All experiments were conducted in at least triplicate to ensure reproducibility.

To evaluate the effect of CystAm modification on enzyme retention and elution from the gold electrode surface, 150 µL of buffer (pH 5.5) was applied to QCM crystals modified with Tyr-CS biosensing layers and incubated for 30 min. This was followed by a rinse with DI-water to remove any detached components. The crystals were then dried at 40 °C for 20 min prior to frequency shift measurements.

The retained masses of the Tyr-CS biosensing layers on both unmodified and CystAm-modified gold electrodes were subsequently compared.

### 2.5 Electrochemical studies

All electrodes with Tyr-CS biosensing layers were subjected to cyclic voltammetry (CV) measurements, regardless of prior CystAm treatment. The measurements were conducted using a one-channel PalmSens4 potentiostat (PalmSens, Utrecht, The Netherlands) at a scan rate of 50 mV/s within a potential window ranging from − 0.4 to 0.1 V [18, 19], unless otherwise specified. Briefly, 150 µL of the test solution was dispensed onto the surfaces of the counter, reference, and working electrodes under ambient conditions (i.e., in the presence of oxygen).

Signal read-out for the calibration of electrodes containing the Tyr–CS biosensing layer was conducted at − 0.1 V. The specificity of the electrodes was evaluated in amperometric (AM) mode using the droplet approach, at − 0.1 V vs. Ag/AgCl reference electrode.

To maximize Tyr activity (the enzyme exhibits optimal catalytic performance in slightly acidic environments, typically around pH 5–6), preserve the integrity of the biosensor layer (as chitosan is more stable and adhesive at acidic pH), and minimize the non-enzymatic degradation of DA, the prepared electrodes were operated at pH 5.5 ± 0.2.

pH measurements were performed using a HORIBA LAQUATWIN PH-22 pH meter (MMM tech support, Berlin, Germany).

### 2.6 Model electrochemical experiments using non-modified and CystAm-modified gold electrodes in redox reactions involving a substrate and the enzymatic reaction product

The copper-dependent enzyme Tyr catalyzes the oxidation of catechols to corresponding quinones (Fig. S2, ESI). Therefore, the electroanalytical performance of non-modified and CystAm-modified gold electrodes in redox reactions with dopamine (DA, the substrate) and dopamine-quinone (DQ, the enzymatic product formed after interaction with Tyr) was compared using CV mode (see Sect. 2.5). To this end, a droplet of standard DA solution (10 µM) was placed on the surface of tested electrode, followed by CV read-out.

To prepare the DQ solution, 10 µL of Tyr was added to a 150 µL droplet of DA in an Eppendorf tube, allowing the reaction to proceed for 100 s (for details see Sect. 2.9). The resulting enzymatic product (DQ) was applied to the surface of electrodes, and the obtained CV profiles were compared with those obtained for DA (Sect. 3.2).

### 2.7 Scanning electron microscopy (SEM)

The morphology of the unmodified and CystAm-modified electrodes was investigated on an FEI Quanta 400 FEG Scanning Electron Microscope (SEM). Back-scattered electron (BSE) images were acquired at 10 kV accelerating voltage using a solid-state detector.

### 2.8 X-ray photoelectron spectroscopy (XPS analysis)

XPS analysis was performed to characterize the surface chemistry of the gold electrodes, irrespective of the pretreatment applied. Measurements were carried out using a photoelectron spectrometer (ESCALAB Mk II, Vacuum Generators) equipped with an Al/Mg twin anode. Al Kα radiation (photon energy: 1486.6 eV, non-monochromatized) was used as the excitation source. High-resolution spectra were acquired with a pass energy of 50 eV, a step size of 0.1 eV, and an energy window of 20 eV. All measurements were conducted in normal emission geometry, with the detector aligned parallel to the surface normal. The S2p spectra were fitted using three spin-orbit doublet components, with the energy separation between two Gaussian components fixed at 1.2 eV. Thiol formation was evaluated by monitoring the $S2p_{3/2}$ signal in the binding energy range of 163.9 eV–165.1 eV.

For stoichiometric analysis, spectral backgrounds were corrected using a linear background subtraction. Measured signal intensities (peak areas above the background) were normalized to the photon flux and further corrected using photoemission cross-sections according to Yeh and Lindau [20, 21].

### 2.9 Oxygen mini-sensor studies

To investigate the effect of CystAm modification on the surface chemistry of gold electrodes, particularly regarding oxygen interactions, an oxygen mini-sensor was employed. Oxygen consumption was evaluated by monitoring the

oxygen concentration (µmol/L) within a droplet of background electrolyte or DA solution placed on the gold electrode surface using an OXR430 needle oxygen mini-sensor (Pyro Science GmbH, Aachen, Germany) [22]. All experiments were performed under ambient conditions at 22 ± 2 °C. Measurement protocols were optimized based on our previous studies [23–27].

An oxygen mini-sensor was also employed to assess the biochemical activity of Tyr in reactions with DA. Since Tyr requires molecular oxygen to catalyze the oxidation of DA (ESI, Fig. S2) [28, 29], monitoring oxygen consumption in solution during the interaction between the enzyme and the substrate provides a means to visualize enzymatic activity and estimate the reaction time. The reaction between DA and added Tyr in solution was completed in approximately 80–100 s (ESI, Fig. S3).

### 2.10 Electrospray ionization mass spectrometry (ESI-MS)

To assess the differences in low molecular weight end-products formed during the transformation of DA *via* gold electrocatalysts (electrochemical route) in comparison with Tyr (biochemical route; see ESI, Fig. S2), ESI-MS analysis was performed.

For the evaluation of end-products formed *via* the electrochemical route, a 150 µL droplet of DA was placed on the surface of gold SPE and subjected to microelectrolysis at 0.1 V for 3600 s. The collected droplet was then injected into the ESI-MS system at a flow rate of 5 µL/min using an acetonitrile/water mixture (50/50, *v/v*).

The analysis was performed using ultra-high-resolution EIC-ESI-MS spectra (Bruker SolariX 7 Tesla ESI/FTICR, Bremen, Germany). Data acquisition was carried out using Bruker's imaging MS software.

## 3 Results and discussion

### 3.1 Characterization of CystAm-modified electrodes

Cysteamine modification is considered a "soft" treatment that helps avoid drastic structural changes to the material. As expected, the morphology of the CystAm-treated gold electrode remained very similar to that of the untreated counterpart (ESI, Fig. S4). However, despite their comparable morphology, the surface chemistry of the non-modified and CystAm-modified gold electrodes showed significant differences.

Thus, XPS analysis confirmed the formation of Au–SH bonds on the surface of the CystAm-modified electrode (Fig. 1, left, red spectrum). Typically, binding energies in the range of 163.9–165.1 eV for the S2p core levels are associated with thiol groups (–SH), with the exact value depending on the local chemical environment [30]. In contrast, for the non-modified gold electrode, only signals corresponding to the Au 4f core levels were observed (Fig. 1, right, black spectrum). In both cases, the Au 4f region exhibited a doublet at approximately 84.0 eV and 87.3 eV, indicating the presence of $Au^0$ [31–33].

Notably, the overall signal intensity corresponding to gold on the surface of the CystAm-treated electrode was several-fold lower compared to the non-modified gold electrode (Fig. 1, right; see also ESI, Table S1). This reduction suggests partial surface blocking by thiol compounds of the CystAm-treated electrode, which may facilitate more

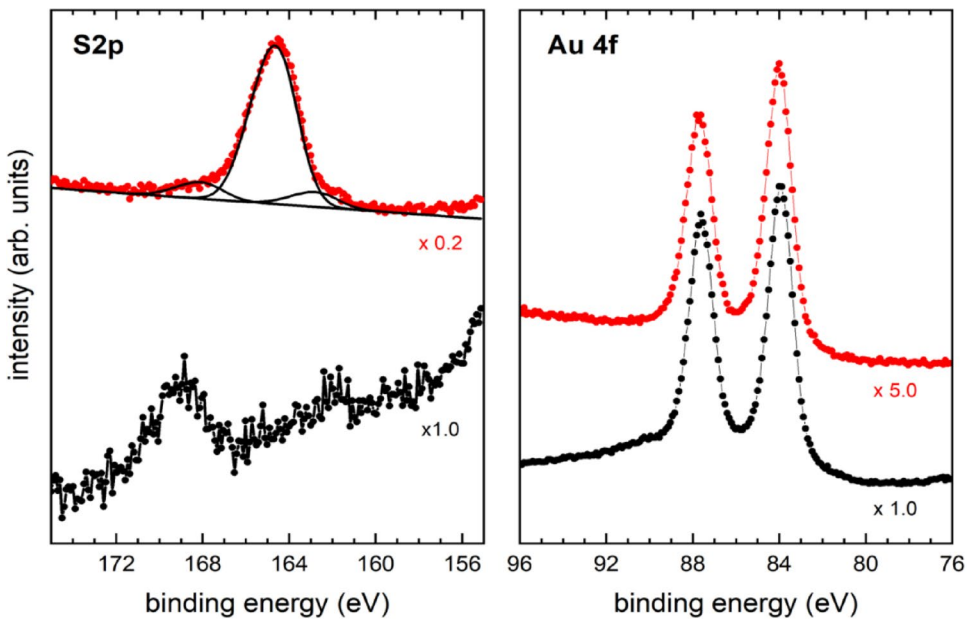


**Fig. 1** XPS spectra recorded from the non-modified (*bottom spectrum*) and CystAm-modified (*top spectrum*) gold SPEs

efficient attachment of the Tyr-CS biosensing layer (see Sect. 3.3). Conversely, the altered surface chemistry resulting from CystAm modification could significantly impact the electrode's electrocatalytic activity in redox reactions. Therefore, even in the absence of the Tyr-CS biosensing layer, differences in electrochemical behavior and oxygen interaction are expected between the non-modified and CystAm-modified gold electrodes.

The subsequent electrochemical studies supported this assumption. Cyclic voltammetry (CV) measurements conducted in a background electrolyte over the potential range of −0.4 V to 0.1 V revealed a distinct difference between the non-modified gold electrode and its CystAm-modified analogue (Fig. 2A). For the non-modified electrode, a pronounced cathodic wave was observed throughout the cathodic range, indicating the oxygen reduction reaction (ORR) occurring at the gold surface (Fig. 2A, *dashed line*). In contrast, this cathodic response was absent following CystAm modification (Fig. 2A, *solid line*), suggesting effective surface passivation.

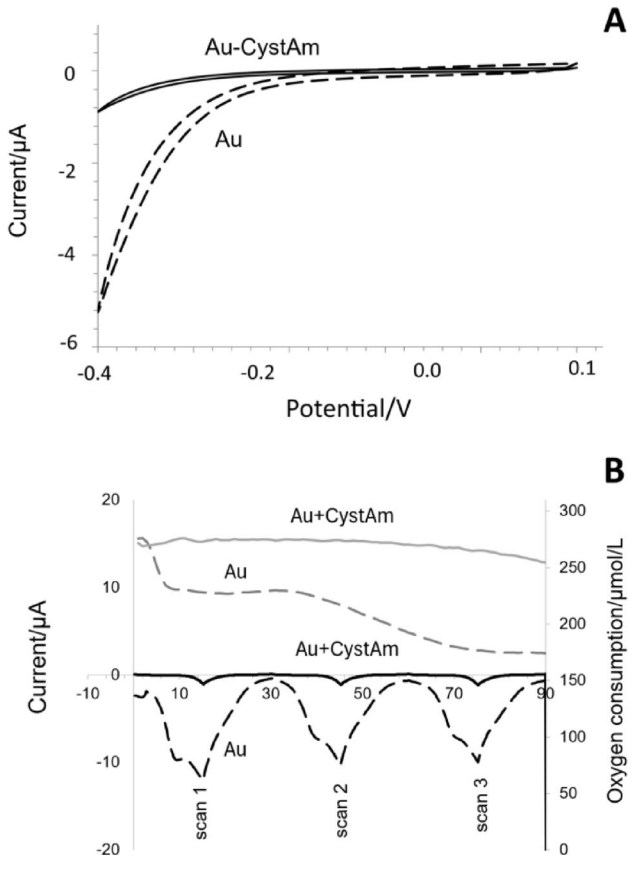


**Fig. 2** CV plots (second scans shown) of the non-modified (*dashed line*) and CystAm-modified (*solid line*) gold (Au) electrodes recorded in a droplet of background electrolyte at 50 mV/s *vs* Ag/AgCl (**A**). Overlaid oxygen and electrochemical (three CV cycles from −0.4 to 0.1 V, scan rate 50 mV/s) responses recorded in a droplet of background electrolyte from the non-modified (*dashed line*) and CystAm-modified (*solid line*) gold electrodes (**B**)

A different oxygen behavior was also observed using an oxygen mini-sensor placed in a droplet of background solution on the electrode surface under applied polarization (Fig. 2B). Oxygen consumption at the surface of the CystAm-modified electrode (Fig. 2B, *grey solid line*) was minimal compared to that of the non-modified gold electrode (Fig. 2B, *grey dashed line*). The baseline oxygen concentration at 20 ± 2 °C was approximately 270 ± 20 µmol/L, with no significant change detected at the CystAm-modified electrode surface. In contrast, oxygen consumption at the non-modified gold electrode increased progressively with each scan, reaching approximately 160 ± 20 µmol/L by the end of the test.

Regarding electrochemical behavior, significantly lower current responses were recorded for the CystAm-modified gold electrode (Fig. 2B, *black solid line*) compared to the unmodified electrode (Fig. 2B, *black dashed line*), indicating reduced oxygen interaction at the modified gold surface.

Whereas the suppression of the ORR by thiol modification, especially via self-assembled monolayers (SAMs) on gold electrodes has been reported in several studies, and the mechanism is generally attributed to physical blocking of oxygen access, changes in surface energy, or impeded electron transfer [34–36], this effect has not been investigated in the context of redox reactions involving electroactive compounds such as DA.

Therefore, the performance of both non-modified and CystAm-modified gold electrodes, along with the reduced effect of ORR, was subsequently compared in redox reactions involving DA, as detailed in the following sections.

## 3.2 The impact of CystAm modification of gold electrodes on their electrochemical performance

The ORR on gold electrodes proceeds with lower efficiency in acidic media compared to alkaline conditions [37–39]. However, under slightly acidic pH, the ORR on gold follows a two-electron pathway, producing hydrogen peroxide ($H_2O_2$) as a byproduct. Concurrently, at acidic pH, $H_2O_2$ can react with DA, leading to the formation of DQ and other oxidized DA species, including indoles, hydroxydopamine and aminochrome [40, 41].

To clarify the processes occurring in the tested systems, next, the electroanalytical performance of both gold electrodes was investigated in model CV experiments using DA and its enzymatic product, DQ, as redox-active analytes.

Interestingly, the unmodified gold electrode, which remained active in the ORR (see Fig. 2A, *dashed line*), exhibited a cathodic response to a low concentration of DA (10 µM), as shown in Fig. 3A (*see CV plot (b) in comparison with (a) obtained for the buffer*). An increase in cathodic current within the signal read-out potential range

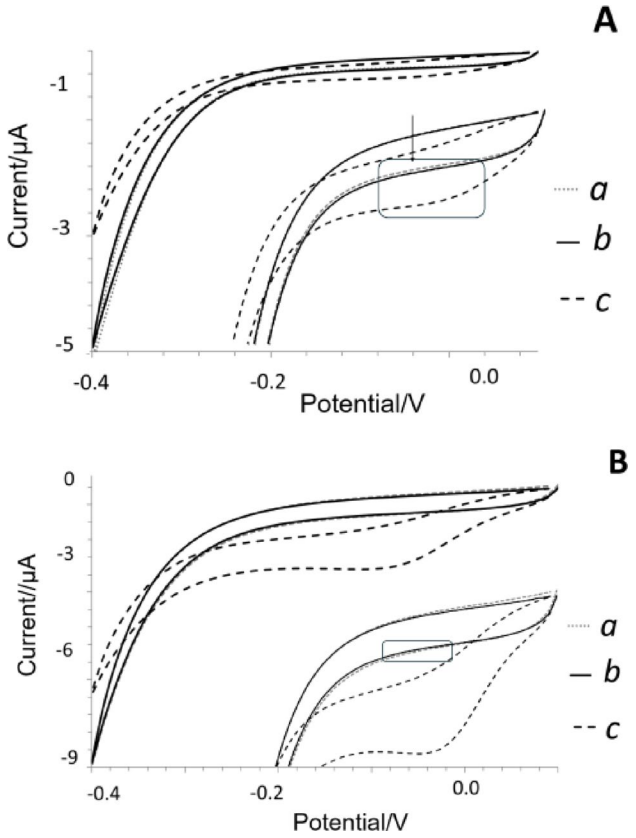


**Fig. 3** CV plots (second scans shown) recorded at 50 mV/s from the non-modified (**A**) and CystAm-modified (**B**) gold electrodes *vs*. Ag/AgCl in a droplet of background electrolyte (*a*), 10 µM DA (*b*) and 10 µM of dopamine-quinone (DQ) (*c*). *Note* The inset (boxed region) highlights the signal read-out area. In (**A**), the arrow indicates an increase in cathodic current corresponding to the presence of DA. The pH of solutions was 5.5 ± 0.2

is highlighted by an arrow. This electrode also responded to DQ, the enzymatic oxidation product of DA catalyzed by Tyr (Fig. 3A, *CV plot* (*c*)).

These observations suggest that, when Tyr is immobilized on the gold electrode surface, several concurrent and potentially interfering processes may occur within the cathodic potential range: (i) intense oxygen reduction reaction (ORR); (ii) spontaneous electrochemical transformation of free DA via a non-enzymatic route, supported by ORR and $H_2O_2$ formation; and (iii) electroreduction of DQ, the enzymatic oxidation product of DA.

Meanwhile, the electrochemically driven transformation of DA (accompanied by the ORR and formation of $H_2O_2$) often results in the formation of aminochrome, which can interfere with the accurate quantification of DA by enzymatic reactions (biochemical route; see ESI, Fig. S5). The formation of aminochrome during the electrochemical process (in the absence of enzyme Tyr) was confirmed by ESI-MS analysis. Specifically, aminochrome was detected at *m/z* 150.05497, corresponding to $[M+H]^+$ (ESI, Fig. S6, *top*), as a characteristic product of electrochemical DA transformation.

In contrast, the CystAm-modified gold electrode did not exhibit a detectable response to the same concentration of DA (10 µM), as shown in Fig. 3B (CV plots (*a*) and (*b*)). Consequently, the formation of aminochrome is not expected under these conditions (ESI, Fig. S6, *bottom*). Notably, the response of the CystAm-modified electrode to the enzymatic product DQ was significantly more pronounced (Fig. 3B, *CV plot* (*c*)) compared to that of the non-modified gold electrode (Fig. 3A, *CV plot* (*c*)). This suggests that the absence of ORR on the CystAm-modified electrode surface prevents the spontaneous electrochemical transformation of free DA, while simultaneously enhancing selectivity and sensitivity toward DQ reduction.

To verify this assumption, we heated the gold electrode at 70 °C for 20 min to enhance its ORR activity. Subsequent electrochemical tests using DA revealed a simultaneous increase in the cathodic current toward DA from the heated electrode (Fig. 4A, CV plot (*a*)) compared to both non-modified and CystAm-modified gold electrodes (Fig. 4A, plots (*b*) and (*c*)).

Moreover, the gold electrode heated to 70 °C exhibited significantly higher oxygen consumption in a 10 µM DA solution, reaching values of 120–150 µmol/L (Fig. 4B, *curve a*), compared to both the non-modified (non-heated) and CystAm-modified gold electrodes (Fig. 4B, *curves b and c*).

These experiments confirm an interfering process between the ORR activity and the DA redox reaction on the gold surface. Specifically, within the cathodic read-out potential range, the intense ORR leads to the formation of $H_2O_2$, which drives the spontaneous electrochemical transformation of free DA *via* a non-enzymatic pathway (Fig. 3A). Altogether, this negatively impacts the accuracy of DA quantification based on the enzymatic (biochemical) reaction following enzyme immobilization on the same electrode. Under these conditions, DA may undergo conversion *via* both electrochemical (*i*) and biochemical (*ii*) pathways, a scenario that should be avoided to ensure selective enzymatic detection of the target subtract.

More importantly, simple modification of the gold electrode with CystAm, which reduces its activity in the ORR, is expected to improve specificity of enzymatic biochemical DA sensing (see Sect. 3.4).

### 3.3 Study of the impact of CystAm modification on the overall architecture of the LbL biosensing layer

CystAm is widely regarded as a "cross-linker" between the electrode surface and the functional biosensing layer, influencing both the crystallization behavior and the

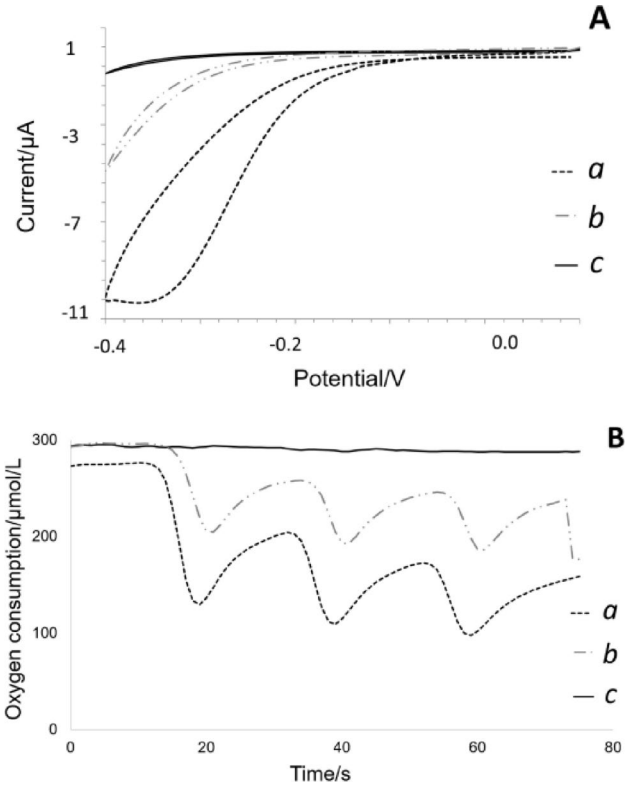


**Fig. 4** CV plots (**A**) (second scans shown) recorded *vs.* Ag/AgCl from the gold electrodes at 50 mV/s in a droplet of 10 μM DA and dynamic oxygen mini-sensor (**B**) responses obtained from: (*a*) non-modified gold electrode heated at 70 °C for 20 min; (*b*) non-modified intact gold electrode; (*c*) CystAm-modified gold electrode. *Note* Oxygen mini-sensor measurements were performed under applied polarization in CV mode (three cycles)

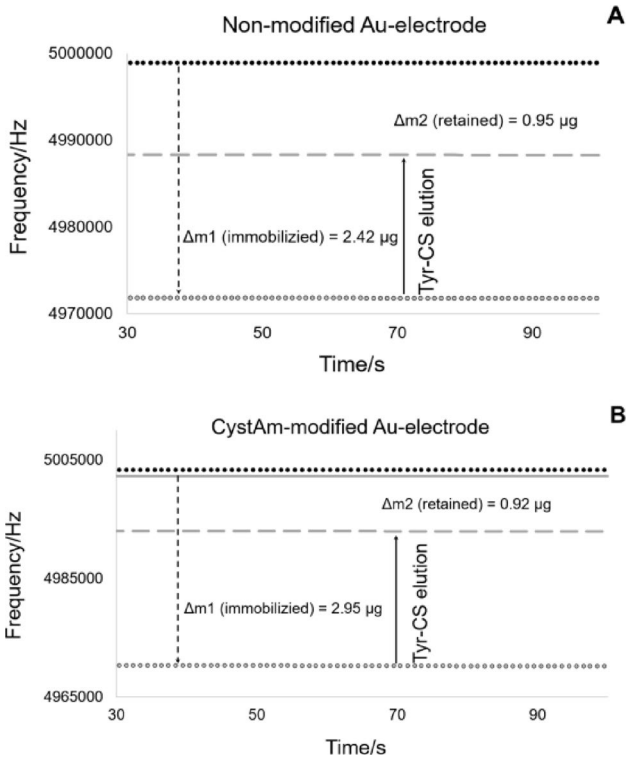


**Fig. 5** QCM frequency response curves recorded after immobilization of the Tyr-CS biosensing layer and its elution from (**A**) non-modified and (**B**) CystAm-modified gold QCM crystals. *Note*: prior measurements, the crystals with the immobilized layers were carefully rinsed with DI-water

architecture of the assembled functional layer [10, 15, 42]. CystAm treatment is expected to alter the packing density and molecular orientation of the biosensing layer, as well as affect key parameters such as the amount of immobilized or retained enzyme, the interaction with substrate and product molecules, and the efficiency of electron transfer pathways ultimately impacting the overall performance of the LbL biosensor/electrode.

To clarify this aspect, potential differences in the architecture of LbL biosensing layers formed on the non-modified and CystAm-modified gold electrodes were analysed by SRS QCM200 system. Mass changes, nanogram-level sensitivity, were monitored at each step of the biosensing layers preparation (see Sect. 2).

Briefly, the application of equal volumes (3 μL) of both the enzyme (Tyr) and the protective polymer agent (chitosan, CS), the total immobilized mass (Δm1) of the biosensing layer on both the unmodified and CystAm-modified gold electrodes did not exceed 3 μg, see Fig. 5 (*indicated by dashed arrows*) and Table S2, ESI.

Unexpectedly, although the frequency changes recorded for the CystAm-modified gold electrode (Fig. 5B, *solid grey line*) confirmed successful surface chemistry modification (see also Figs. 1 and 2), no significant additional frequency shifts were observed following immobilization of the biosensing layer (Tyr-CS), as compared to the non-modified gold electrode. These results suggest that the amount of immobilized biosensing layer by physical adsorption on the non-modified gold electrode was nearly identical to that on the CystAm-modified analogue (ESI, Table S2, Δm1; 2.62 ± 0.18 μg for the unmodified electrode vs. 2.71 ± 0.26 μg for the CystAm-modified electrode).

Although CystAm treatment is often considered a more robust immobilization strategy than physical adsorption due to its presumed ability to reduce component leakage during use [11, 43], subsequent elution tests did not support this assumption. Specifically, QCM analysis revealed no improvement in the retained mass of the Tyr-CS biosensing layer following elution tests (ESI, Table S2, Δm2: 1.14 ± 0.17 μg for the unmodified electrode vs. 0.76 ± 0.14 μg for the CystAm-modified electrode), see also Fig. 5 (solid arrows). These results suggest that CystAm modification of gold electrodes does not significantly influence the

architecture of the biosensing layer, specifically in terms of packing density, retained mass, or elution rates.

At the same time, it is widely accepted [10–12] that CystAm treatment of gold electrode helps preserve the immobilized enzyme in a favorable conformation, thereby supporting its retained biochemical activity and enabling effective catalytic function and interaction with the target analyte.

To verify this aspect, the retained enzymatic activity was compared between two electrodes, each with immobilized biosensing layers. For this goal, an oxygen mini-sensor was positioned directly above the working electrode surface in a droplet of 10 µM DA solution. Since the biochemical activity of Tyr involves molecular oxygen consumption (see ESI, Figs. S2, S3 for details), dynamic monitoring of oxygen concentration at the electrode surface upon contact with the target substrate (DA) enables evaluation of the enzyme's biochemical activity. This approach provides direct comparison of enzymatic performance as a function of electrode design and surface chemistry (i.e., non-modified vs. CystAm-modified gold electrodes).

Interestingly, oxygen consumption at the surface of the working electrode with an immobilized biosensing layer was nearly identical for both systems (ESI, Fig. S7). In brief, no enhancement in enzymatic activity was observed for Tyr immobilized on the CystAm-modified gold electrode. Consequently, it can be concluded that the efficiency of Tyr-CS biosensing layer immobilization on gold electrodes appears to be independent of CystAm surface modification.

## 3.4 Effect of CystAm modification of gold electrocatalysts on the electroanalytical performance of LbL-constructed biosensors in biochemical reactions with DA

### 3.4.1 Performance in model solutions

Next, the electroanalytical performance of both electrode systems (non-modified and CystAm-modified) with immobilized Tyr-CS biosensing layers was compared using model solutions containing DA.

Notably, the CystAm-modified electrode with the immobilized Tyr-CS biosensing layer demonstrated superior sensitivity, an extended linear dynamic range (LDR), and a limit of quantification (LOQ) for DA concentrations above 5 µM, Table 1.

Briefly, CystAm modification of the gold electrode nearly doubled the sensitivity for enzymatic DA determination above 5 µM compared to the non-modified electrode. Additionally, the limit of quantification (LOQ) was reduced by a factor of 2.5. Since the amount of Tyr-CS biosensing layer was identical in both electrode designs (see Sect. 3.3), these improvements in analytical performance are attributed primarily to changes in the surface chemistry of the gold electrocatalytic layer. More specifically, CystAm treatment induces the formation of thiol bonds, which deactivate the gold electrodes toward the ORR. This deactivation correlates with reduced electrocatalytic activity of the gold electrode for the cathodic reduction of free DA to DQ, thereby enhancing the selectivity and sensitivity toward enzymatic DA detection (biochemical route).

At very low DA concentrations (0.5–5 µM), the Tyr-CS CystAm-modified gold electrode exhibited only minor improvements in sensitivity and regression coefficient, resulting in limited overall enhancement of analytical performance. Nonetheless, even these modest gains observed in model systems may prove significant when analyzing DA in complex biological matrices (see Sect. 3.4.2).

Specificity tests of the fabricated gold electrodes with the immobilized biosensing layers revealed a slight improvement in the performance of the CystAm-modified electrode. Notably, the CystAm-modified electrode with the Tyr-CS immobilized biosensing layer showed no response to electroactive interferents such as L-lactate and glucose, whereas the non-modified electrode exhibited measurable responses, Fig. 6.

In summary, modulating the surface chemistry and catalytic properties of the gold electrocatalyst *via* CystAm treatment allows for tuning the sensitivity and overall electroanalytical performance of amperometric biosensors with immobilized Tyr-CS biosensing layer, while simultaneously enhancing specificity without altering the biosensing components.

**Table 1** Electroanalytical performance of non-modified and CystAm-modified gold electrodes with immobilized Tyr-CS biosensing layers in DA model solutions at pH 5.5 ± 0.2

| System | Calibration formula | $R^2$ | Sensitivity/µA µM$^{-1}$ cm$^{-2}$ [a] | LDR/µM | LOQ/µM |
|---|---|---|---|---|---|
| Tyr-CS based on non-modified Au | y = − 0.066·x − 0.1275 | 0.9943 | 0.5250 | 0–5 | 0.5 |
| | y = − 0.0083·x − 0.1215 | 0.8868 | 0.0660 | 0–15 | 5 |
| Tyr-CS based on CystAm-modified Au | y = − 0.0746·x − 0.0631 | 0.9966 | 0.5935 | 0–5 | 0.5 |
| | y = − 0.0128·x − 0.0316 | 0.9794 | 0.1018 | 0–15 | 2 |

Signal read-out was conducted at − 0.1 V

[a]Electrode surface area was 0.1257 cm$^2$

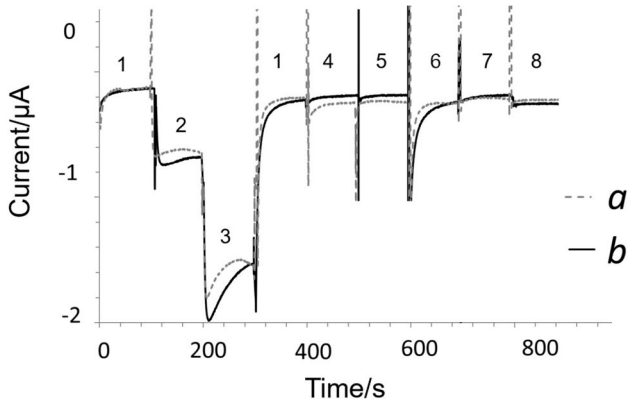


**Fig. 6** Specificity tests recorded in AM mode at − 0.1 V from the non-modified (*a*) and CystAm-modified (*b*) gold electrodes with the Tyr-CS immobilized layers. Measurements were conducted by dropping the following solutions onto the electrode surface: (*1*) background buffer solution, (*2*) 5 µM dopamine (DA), (*3*) 10 µM DA, (*4*) 1 mM L-lactate, (*5*) 1 mM glucose, (*6*) 20 µM hydrogen peroxide ($H_2O_2$), (*7*) 50 µM ascorbic acid (AA), (*8*) 10 µM hydroquinone (HQ). *Note* The pH of all test solutions was 5.5 ± 0.2. The experiments were conducted in triplicate and yielded the same results.Since the content and composition of the Tyr-CS biosensing layer including the type and amount of immobilized enzyme remain constant (see Fig. 5), the observed effects can be exclusively attributed to the altered properties of the electrocatalyst, specifically the CystAm-modified gold electrode and its deactivation in the ORR (see Sect. 3.1)

**Table 2** Selected recovery data for DA determination in saliva using unmodified and CystAm-modified gold electrodes with immobilized Tyr-CS biosensing layers

| Electrode/calibration formula | Added DA/µM | Found DA/µM | Recovery/% | RSD/% |
|---|---|---|---|---|
| Tyr-CS based on unmodified Au<br>$y = -0.0442x - 0.0812$<br>$R^2 = 0.992$ | 0.5 | 0.45 ± 0.005 | 90.0 | 5.91 |
| | 1 | 0.70 ± 0.01 | 70.8 | 8.80 |
| | 2 | 1.88 ± 0.03 | 94.0 | 15.0 |
| Tyr-CS based on CystAm-modified Au<br>$y = -0.0593x - 0.1407$<br>$R^2 = 0.998$ | 0.5 | 0.49 ± 0.005 | 98.8 | 3.25 |
| | 1 | 0.99 ± 0.01 | 99.0 | 8.42 |
| | 2 | 2.01 ± 0.02 | 100.5 | 8.9 |

### 3.4.2 Determination of DA in artificial saliva

Next, the electroanalytical performance of both electrode systems was evaluated for DA determination in artificial saliva solutions (as a case study), a relevant biological matrix. The analytically significant concentration range of DA in saliva typically falls within the low micromolar range. Fusayama/Meyer artificial saliva (pH 5.2 ± 0.2) was spiked with known concentrations of DA, followed by electrochemical analysis using gold electrodes with immobilized Tyr-CS biosensing layer. Particular focus was placed on the physiologically relevant low concentration range of DA (0.5–2 µM) [3, 4, 6]. Selected quantification results for DA in artificial saliva are summarized in Table 2. The corresponding calibration plots are provided in ESI, Fig. S8.

As expected, the CystAm-modified electrode with the immobilized Tyr-CS layer demonstrated superior electrocatalytic performance for DA quantification in artificial saliva. This improvement is likely due to the absence of interfering ORR on the gold electrode surface and minimized electrochemical reduction of free DA via non-enzymatic pathways. Average recovery rates for saliva samples were 99% and 100%, with relative standard deviations (RSD) below 10%.

Although the RSD values obtained in this study for the CystAm-modified electrode did not exceed 10%, it is anticipated that replacing the current LbL architecture with an electrodeposition-based immobilization method for Tyr and chitosan [44, 45] could significantly enhance electrode-to-electrode reproducibility of the amperometric biosensors. This optimization is planned for future investigations in our laboratory.

## 4 Conclusions

This study investigated the role of CystAm modification of gold electrodes in both electrochemical (i) and biochemical (ii) reactions involving dopamine (DA). Using XPS, CV, and oxygen mini-sensor studies, we found that CystAm treatment significantly suppresses the oxygen reduction reaction (ORR), reducing hydrogen peroxide formation and thus limiting non-enzymatic DA transformation under acidic conditions.

In contrast, QCM data showed that CystAm had minimal effect on Tyr immobilization, retention, elution, or enzymatic activity, leaving the biosensing layer architecture largely unchanged. Therefore, the enhanced electroanalytical performance of LbL enzymatic DA biosensors was attributed solely to the altered electrocatalytic properties, particularly ORR suppression of the CystAm-modified gold electrocatalyst. This highlights the potential of tuning electrode surface chemistry, rather than the biosensing layer, to improve biosensor specificity and performance.

The results obtained in this study provide a framework for controlled and tunable surface chemistry of biosensing layers based on gold electrocatalysts, Tyr, and chitosan, used for enzymatic DA detection. The knowledge gained can potentially be extended to enable reliable electroanalysis of other neurotransmitters in the future.

**Supplementary Information** The online version contains supplementary material available at https://doi.org/10.1007/s10800-025-02378-y.

**Acknowledgements** The authors would like to thank Dr. Nuriye Korkmaz (KIST Europe, Saarbrücken, Germany) for the SEM studies of gold screen printed electrodes, Dr. Peter König (INM – Leibniz

Institute for New Materials, Saarbrücken, Germany) for performing of the stability tests of the intact CystAm solution and PD.Dr. Frank Müller (Saarland University, Experimental Physics, Saarbrücken, Germany) for the conducted XPS investigations.

**Author contributions** H. Caparrotti: Formal analysis, investigation, methodology, data acquisition, validation; Y.E. Silina: Conceptualization, data acquisition, funding acquisition, analysis, validation, writing –original draft.

**Funding** Open Access funding enabled and organized by Projekt DEAL. This study was a part of the research program of Y.E.S. funded by the Deutsche Forschungsgemeinschaft (DFG, German Research Foundation, Project 427949628).

**Data availability** No datasets were generated or analysed during the current study.

## Declarations

**Competing interests** The authors declare no competing interests.



## References

1. Caligiore D, Giocondo F, Silvetti M (2022) The neurodegenerative elderly syndrome (NES) hypothesis: alzheimer and Parkinson are two faces of the same disease. IBRO Neurosci Rep 13:330–343. https://doi.org/10.1016/j.ibneur.2022.09.007
2. Riederer P, Horowski R (2023) l-DOPA-therapy in Parkinson's disease: some personal reflections on l-DOPA therapy from Vienna and Berlin. J Neural Transm 130:1323–1335. https://doi.org/10.1007/s00702-023-02692-9
3. Gonzalez-Sepulveda M, Laguna A, Carballo-Carbajal I et al (2020) Validation of a reversed phase UPLC-MS/MS method to determine dopamine metabolites and oxidation intermediates in neuronal differentiated SH-SY5Y cells and brain tissue. ACS Chem Neurosci 11:2679–2687. https://doi.org/10.1021/acschemneuro.0c00336
4. Lin Y, Spiller K, Aras R, Jian W (2022) UPLC-MS/MS assay for the simultaneous determination of catecholamines and their metabolites at low pg/mg in rat/mouse striatum. J Pharm Biomed Anal 213:114697. https://doi.org/10.1016/j.jpba.2022.114697
5. Sun F, Zhou J, Dai B et al (2020) Next-generation GRAB sensors for monitoring dopaminergic activity in vivo. Nat Methods 17:1156–1166. https://doi.org/10.1038/s41592-020-00981-9
6. Liu X, Liu J (2021) Biosensors and sensors for dopamine detection. VIEW 2:20200102. https://doi.org/10.1002/VIW.20200102
7. Mondal R, Mukherjee N, Ahmed SF (2025) A comprehensive review on the enzyme-free electrochemical dopamine sensing: development and challenges since inception. Inorg Chem Commun 178:114449. https://doi.org/10.1016/j.inoche.2025.114449
8. DeVoe E, Andreescu S (2024) Review—Catalytic electrochemical biosensors for dopamine: design, performance, and healthcare applications. ECS Sens Plus. https://doi.org/10.1149/2754-2726/ad3950
9. Bounegru AV, Apetrei C (2023) Tyrosinase immobilization strategies for the development of electrochemical biosensors—a review. Nanomaterials. https://doi.org/10.3390/nano13040760
10. Roushani M, Valipour A, Valipour M (2016) Layer-by-layer assembly of gold nanoparticles and cysteamine on gold electrode for Immunosensing of human chorionic gonadotropin at picogram levels. Mater Sci Eng C 61:344–350. https://doi.org/10.1016/j.msec.2015.12.088
11. Hernández HD, Dominguez RB, Gutiérrez JM (2024) Screen-printed carbon electrode functionalized with AuNPs-cysteamine self-assembled monolayers for enzymatic uric acid detection in non-invasive samples. Sens Bio-Sensing Res. https://doi.org/10.1016/j.sbsr.2024.100677
12. Atallah C, Charcosset C, Greige-Gerges H (2020) Challenges for cysteamine stabilization, quantification, and biological effects improvement. J Pharm Anal 10:499–516. https://doi.org/10.1016/j.jpha.2020.03.007
13. Michota A, Kudelski A, Bukowska J (2000) Chemisorption of cysteamine on silver studied by surface-enhanced Raman scattering. Langmuir 16:10236–10242. https://doi.org/10.1021/la000707z
14. Pandey P, Pandey A, Shukla NK (2018) Screen printed gold electrode with cysteamine and single walled carbon nanotubes for the recognition of prostate specific antigen. Mater Today Proc 5:15311–15318. https://doi.org/10.1016/j.matpr.2018.05.011
15. Giancarla A, Zanoni C, Merli D et al (2024) A new cysteamine-copper chemically modified screen-printed gold electrode for glyphosate determination. Talanta 269:125436. https://doi.org/10.1016/j.talanta.2023.125436
16. Mogilevsky CS, Lobba MJ, Brauer DD et al (2021) Synthesis of multi-protein complexes through charge-directed sequential activation of tyrosine residues. J Am Chem Soc 143:13538–13547. https://doi.org/10.1021/jacs.1c03079
17. Hu J, Huang X, Xue S et al (2020) Measurement of the mass sensitivity of QCM with ring electrodes using electrodeposition. Electrochem Commun 116:106744. https://doi.org/10.1016/j.elecom.2020.106744
18. Liu A, Honma I, Zhou H (2005) Electrochemical biosensor based on protein-polysaccharide hybrid for selective detection of nanomolar dopamine metabolite of 3,4- dihydroxyphenylacetic acid (DOPAC). Electrochem Commun 7:233–236. https://doi.org/10.1016/j.elecom.2004.12.015
19. Liu A, Honma I, Zhou H (2005) Amperometric biosensor based on tyrosinase-conjugated polysacchride hybrid film: selective determination of nanomolar neurotransmitters metabolite of 3,4-dihydroxyphenylacetic acid (DOPAC) in biological fluid. Biosens Bioelectron 21:809–816. https://doi.org/10.1016/j.bios.2005.03.005
20. Shirley DA (1972) High-resolution X-ray photoemission spectrum of the Valence bands of gold. Phys Rev B 5:4709–4714
21. Yeh JJ, Lindau I (1985) Atomic subshell photoionization cross sections and asymmetry parameters: $1 \leq Z \leq 103$. Data Nucl Data Table 32:1–155. https://doi.org/10.1016/0092-640X(85)90016-6
22. Semenova D, Silina YE, Koch M et al (2019) Sensors for biosensors: a novel tandem monitoring in a droplet towards efficient screening of robust design and optimal operating conditions. Analyst. https://doi.org/10.1039/c8an02261e

23. Silina YE, Apushkinskaya N, Talagaeva NV et al (2021) Electrochemical operational principles and analytical performance of Pd-based amperometric nanobiosensors. Analyst 146:4873–4882. https://doi.org/10.1039/D1AN00882J
24. Koch M, Apushkinskaya N, Zolotukhina EV, Silina YE (2021) Towards hybrid one-pot/one-electrode Pd-NPs-based nanoreactors for modular biocatalysis. Biochem Eng J 175:108132. https://doi.org/10.1016/j.bej.2021.108132
25. Apushkinskaya N, Zolotukhina EV, Butyrskaya EV, Silina YE (2022) In situ modulation of enzyme activity via heterogeneous catalysis utilizing solid electroplated cofactors. Comput Struct Biotechnol J 20:3824–3832. https://doi.org/10.1016/j.csbj.2022.07.012
26. Butyrskaya EV, Korkmaz N, Zolotukhina EV et al (2021) Mechanistic aspects of functional layer formation in hybrid one-step designed GOx/Nafion/Pd-NPs nanobiosensors. Analyst 146:2172–2185. https://doi.org/10.1039/d0an02429e
27. Semenova D, Gernaey KV, Morgan B, Silina YE (2020) Towards one-step design of tailored enzymatic nanobiosensors. Analyst. https://doi.org/10.1039/c9an01745c
28. Florescu M, David M (2017) Tyrosinase-based biosensors for selective dopamine detection. Sens (Switzerland). https://doi.org/10.3390/s17061314
29. Kanteev M, Goldfeder M, Fishman A (2015) Structure-function correlations in tyrosinases. Protein Sci 24:1360–1369. https://doi.org/10.1002/pro.2734
30. Ahmed MMM, Liao C, Venkatesan S et al (2025) Sulfur-functionalized sawdust Biochar for enhanced cadmium adsorption and environmental remediation: a multidisciplinary approach and density functional theory insights. J Environ Manage 373:123586
31. De Anda Villa M, Gaudin J, Amans D et al (2019) Assessing the surface oxidation state of free-standing gold nanoparticles produced by laser ablation. Langmuir 35:11859–11871. https://doi.org/10.1021/acs.langmuir.9b02159
32. Klyushin AY, Rocha TCR, Hävecker M et al (2014) A near ambient pressure XPS study of Au oxidation. Phys Chem Chem Phys 16:7881–7886. https://doi.org/10.1039/c4cp00308j
33. Gopinath CS, Muthukumaran R, Welling LL et al (1998) X-ray photoelectron spectroscopic studies on binuclear gold(II) complexes. Chem Phys Lett 296:566–570. https://doi.org/10.1016/S0009-2614(98)01089-6
34. El-Deab MS, Ohsaka T (2003) Quasi-reversible two-electron reduction of oxygen at gold electrodes modified with a self-assembled submonolayer of cysteine. Electrochem Commun 5:214–219. https://doi.org/10.1016/S1388-2481(03)00020-1
35. Vago ER, de Weldige K, Rohwerder M, Stratmann M (1995) Electroreduction of oxygen on octadecylmercaptan self-assembled monolayers. Fresenius J Anal Chem 353:316–319. https://doi.org/10.1007/BF00322059
36. Yang L, Wei W, Xia J et al (2005) Electrochemical studies of derivatized thiol self-assembled monolayers on gold electrode in the presence of surfactants. Anal Sci 21:679–684. https://doi.org/10.2116/analsci.21.679
37. Erikson H, Sarapuu A, Kozlova J et al (2015) Oxygen electroreduction on electrodeposited PdAu nanoalloys. Electrocatalysis 6:77–85. https://doi.org/10.1007/s12678-014-0222-1
38. El-Deab MS, Sotomura T, Ohsaka T (2006) Oxygen reduction at Au nanoparticles electrodeposited on different carbon substrates. Electrochim Acta 52:1792–1798. https://doi.org/10.1016/j.electacta.2005.12.057
39. Tripachev O, Bogdanovskaya V, Tarasevich M, Andoralov V (2012) Gold autodeactivation during oxygen electroreduction studied by electrochemical impedance spectroscopy. J Electroanal Chem 683:21–24. https://doi.org/10.1016/j.jelechem.2012.07.030
40. De Iuliis A, Arrigoni G, Andersson L et al (2008) Oxidative metabolism of dopamine: a colour reaction from human midbrain analysed by mass spectrometry. Biochim Biophys Acta Proteins Proteom 1784:1687–1693. https://doi.org/10.1016/j.bbapap.2008.07.002
41. Jaramillo AM, Barrera-Gutiérrez R, Cortés MT (2020) Synthesis, follow-up, and characterization of polydopamine-like coatings departing from micromolar dopamine-o-quinone precursor concentrations. ACS Omega 5:15016–15027. https://doi.org/10.1021/acsomega.0c00676
42. Abbas SS, Kelly NL, Patias G et al (2020) Cysteamine functionalised reduced graphene oxide modification of maleated poly(propylene). Polym (Guildf) 203:122750. https://doi.org/10.1016/j.polymer.2020.122750
43. Cai Q, Xu B, Ye L et al (2014) Immobilization of biomolecules on cysteamine-modified polyaniline film for highly sensitive biosensing. Talanta 120:462–469. https://doi.org/10.1016/j.talanta.2013.11.013
44. Koch M, Silina YE (2024) Uric acid detection by hydrogen peroxide independent biosensors: novel insights and applications. Microchem J 207:112091. https://doi.org/10.1016/j.microc.2024.112091
45. Silina YE (2024) One-step electrodeposited hybrid nanofilms in amperometric biosensor development. Anal Methods 16:2424–2443. https://doi.org/10.1039/d4ay00290c